Molecular Insight into the Cosolvent Effect on Lignin–Cellulose Adhesion

Sonia Milena Aguilera-Segura, Francesco Di Renzo, Tzonka Mineva

Molecular insight into the cosolvent effect on the lignin-cellulose adhesion.

[a]Sonia Milena Aguilera-Segura, [a]Francesco Di Renzo*, [a]Tzonka Mineva*

[a.]ICGM, Univ Montpellier, CNRS, ENSCM, Montpellier, France

* To whom correspondence should be addressed

Emails: Francesco.Di-Renzo@enscm.fr; tzonka.mineva@enscm.fr

Abstract

Understanding and controlling the physical adsorption of lignin compounds on cellulose pulp is a key parameter for a successful optimization of organosolv processes. The effect of binary organic-aqueous solvents on the coordination of lignin to cellulose was studied with molecular dynamics simulations, considering ethanol and acetonitrile as organic co-solvents in aqueous solutions in comparison to their mono-component counterparts. The structures of the solvation shells around cellulose and lignin, as well as the energetics of the lignin-cellulose adhesion, indicate a more effective disruption of lignin-cellulose binding by binary solvents. The synergic effect between solvent components is explained by their preferential interactions with cellulose-lignin complexes. In the presence of pure water, long-lasting H-bonds in the lignin-cellulose complex are observed, promoted by the non-favorable interactions of lignin with water. Ethanol and acetonitrile compete with water and lignin for cellulose oxygen binding sites, causing a non-linear decrease of the cellulose-lignin interactions with the amount of the organic component. This effect is modulated by the water exclusion from the cellulose solvation shell by the organic solvent component. The amount and rate of water exclusion depend on the type of organic cosolvent and its concentration.

Introduction

The promising use of wood, i.e. lignocellulosic biomass, as a next-generation, environmentally sustainable feedstock of organic carbon has prompted an intense search in industry and academia towards economically viable processes for biomass degradation into fuel or chemicals precursors.[1] The complex nature of wood, constructed from a variety of organic polymers of

unique structural and chemical characteristics, renders the selective breakdown of lignocellulosic biomass highly challenging. The skeletal material of wood cell walls is cellulose, a long chain, linear polysaccharide composed of glucose monomers (Figure1A). It accounts for about 40-45 wt% of the dry weight of normal wood tissue. Cellulose is organized into fibrils[2] and interacts with a surrounding matrix formed by hemicellulose and lignin.[3, 4] Lignin, which is the third major constituent of wood after cellulose and hemicelluloses, composes around 25-35 wt% of the total dry weight and plays a major role in preventing buckling of the lignocellulose wall structure.[5] The contribution of lignin to the mechanical properties of wood is also related to the interactions of wood components with a solvent. Indeed, a hydrophobic lining of lignin prevents a weakening of the cohesion of cellulose fibrils upon hydration.[6, 7]

Lignin is a highly branched, heterogeneous polyphenolic polymer, with a complex molecular structure that varies with the source of biomass and isolation method. The modeling of lignin is a considerable challenge due to the lack of a regular and ordered structure. The β-O-4 linkage represents the predominant inter-unit linkage in lignin, and it is a good model for studying major conformation features such as H-bonding and flexibility.[8] We have therefore chosen here to study the guaiacyl (G) β-O-4 dimer (Figure 1B) model compound, majoritarily in softwood.

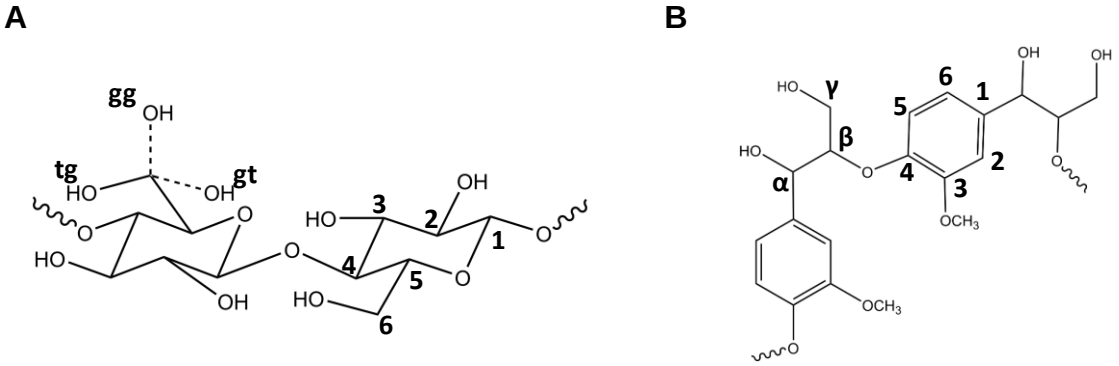

Figure 1 (A) Cellulose cellobiose unit and the three hydroxymethyl group conformers tg (bulk, plain line), gt, and gg (dashed lines) measured from the torsion angles O6-C6-C5-O5 and O6-C6-C5-C4, respectively. Ideal tg, gt, and gg conformations would be characterized by the torsion angle ω (O6-C6-C5-O5) = 180°, 60°, and -60°, respectively.[2] (B) a guaiacyl dimer (G-G) connected with a β-O'-4' linkage.

Disassembling of lignocellulose matter in paper pulping is the major economic activity, enabling the use of renewable resources to satisfy the world needs of more than 400 Mt of paper and cardboard per year.[9] In most current chemical pulping, the only product targeted is oligocellulose and the solubilized lignin fraction is slightly more than a waste, which is only

thermally valorized in the wet combustion process needed to recycle the salts and the aggressive inorganic chemicals used in the pulping process.[10] The introduction of greener processes for disassembling plant biomass remains a major environmental issue, which could allow a better valorization of the rich chemistry of lignin components. The higher purity requirement for cellulose used in second-generation ethanol biorefineries is fostering a development of organosolv pulping processes, favoring the recovery of lignin coproducts.[11-13] In organosolv fractionation of lignocellulosic biomass, wood is in contact with different solvents in order to produce treated fractions of cellulose pulp, soluble lignin, and hemicelluloses-derived products.[14, 15] The use of multi-component solvents has provided remarkable results in fractionation processes of several levels of severity, ranging from swelling, dilute acid, hydrothermal, steam explosion, alkaline treatment, to organosolv pulping.[14-28] Despite all invested efforts, no fractionation method is currently capable of valorizing all functionalities of lignocellulose components in an economically viable commercial-scale deconstruction process.

This has stimulated a significant amount of recent experimental and theoretical investigations of the behavior of lignocellulosic polymers in mono-component solvents,[8, 29-64] shedding light on the microscopic interactions between crystalline or amorphous biopolymers and mono-component solvent. These interactions present a high technological relevance, as a successful pulping process does not only imply the cleavage of bonds between lignocellulosic components but also requires an effective separation of these components by the solvent. Retention of lignin-like compounds on cellulose not only decreases the pulping yield but also significantly affects the surface properties of cellulose fibers, modifying the hydrophilic-hydrophobic balance of the pulp.[65-67] Moreover, retention of lignin has been reported to impair the bio-digestibility of organosolv pulp, a critical parameter in the production of bio-ethanol.[68, 69]

Molecular dynamics (MD) simulations, often in combination with experimental investigations, have provided important insights on several parameters affecting the interactions of lignin with the cellulose surface. Major contributions have been brought into: (i) the orientation of the hydroxymethyl groups of pure crystalline and amorphous cellulose in water, discriminating between the hydrophilic and hydrophobic surfaces of cellulose;[31-40] (ii) the degree of cellulose surface structuring due to water-cellulose hydrogen bonding (HB)[39, 40]; and (iii) the lignin adhesion to cellulose microfibrils,[8, 41, 42, 45, 47-51, 70, 71] highlighting the role of van der Waals (vdW) forces in lignin-cellulose adhesion[41, 51] and the stabilizing effect of internal HB in the absence of external HB in several different dimeric conyferil alcohol structures.[45]

Whereas extensive work on lignocellulosic components (mostly cellulose) in various mono-component solvents has been carried out, only a few computational studies approach the molecular action of co-solvents in multicomponent liquids on the structural properties of lignocellulosic biomass and the interactions between the lignocellulosic polymers.[64, 72-81] Quantum chemical density functional theory-based method augmented with an implicit solvent (COSMO-RF) approach for binary solvent mixtures[82] evidenced the role of anions in the ionic liquids to dissolve lignin and cellulose from the computed excess enthalpies. The explicit treatment of solvent molecules, studied with all-atom MD simulations[72, 73] showed that tetrahydrofuran (THF) - a polar aprotic ether - preferentially solvates lignin, which shifts the equilibrium conformational distribution from a crumpled globule to a coil lignin conformer. Whereas pure water is a bad solvent for lignin, the THF-cosolvent in water facilitates access of cellulolytic enzymes to cellulose.[72] Simulation of glucose solvation in water, THF, DMSO, and DMF[74] showed that the organic solvents compete with water to be in the first solvation shell of glucose and a significant amount of water is pushed to the second solvation shell.

Very recent experimental and atomistic simulations support the observation that lignin dissociates from cellulose in the presence of ethanol[64] and THF solvents.[64, 78-81] Our MD simulations[64] provided the first shreds of evidence that the lignin adsorption on cellulose in pure water solvent is disrupted upon the addition of 50 and 75 wt% ethanol co-solvent in line with the experimentally observed high swelling of wood after immersion in 44 wt% aqueous ethanol solution[64]. Ethanol and other easily recoverable organic solvents in water appear promising solvents for the development of economically viable processes of wood dissolution,[15] because they increase significantly wood deformation and swelling in comparison to their pure components. A high swelling in non-linear relation with the concentration of the organic component (ethanol, acetone, isopropanol, and acetonitrile) has been reported for the range of ~40 – 80 wt% cosolvent concentration.[64, 68] To address the microscopic origin of the effect of organic cosolvents we assess in the present work the evolution of cellulose-lignin interactions in water-ethanol and water-acetonitrile binary solvents at 50 and 75 wt% concentrations, in comparison with the respective mono-component solvents, i.e. water, ethanol, and acetonitrile. This study highlights the role of co-solvent preferential coordination to cellulose surface on lignin adhesion to cellulose. Cosolvent-induced conformational changes and exclusion of water from cellulose solvation shells are other molecular factors that aid the detachment of lignin.

Experimental

Models

The models used in this study consists of a truncated cellulose crystal (called throughout cellulose nanocrystal) and a dimer of guaiacyl (G) monomers. The cellulose nano-crystal was built with seven cellulose chains, eight-monomers long (56 anhydroglucose units, Figure 2A), starting from the crystallographic structure of cellulose $I\beta$[2] and created with the cellulose-builder tool of Gomes and Skaf.[83] Oxygen terminal residues were capped with hydrogen atoms and carbon terminal residues were capped with OH groups to obtain a finite chain. The model reproduces correctly the intramolecular and intermolecular hydrogen bond patterns expected for cellulose Iβ chains.[84] This model is large enough to represent both the hydrophilic and hydrophobic cellulose domains and is small enough to allow for maximum interaction with solvent molecules at both hydrophilic and hydrophobic sites. The terminal oxygen residues of the G-monomers in the lignin dimer are capped with hydrogen atoms (Figure 2B). The G monomers are β-O-4 linked, this being the most frequent linkage found in natural lignin, connecting two units by an ether bond between a β-carbon and a C4 on the phenyl ring. The guaiacyl dimer has four major molecular features, which we consider essential to study the lignin-solvent and cellulose-lignin inter-molecular interactions, namely two aromatic rings, hydroxyl groups, methoxy groups, and β-O-4 linkage.

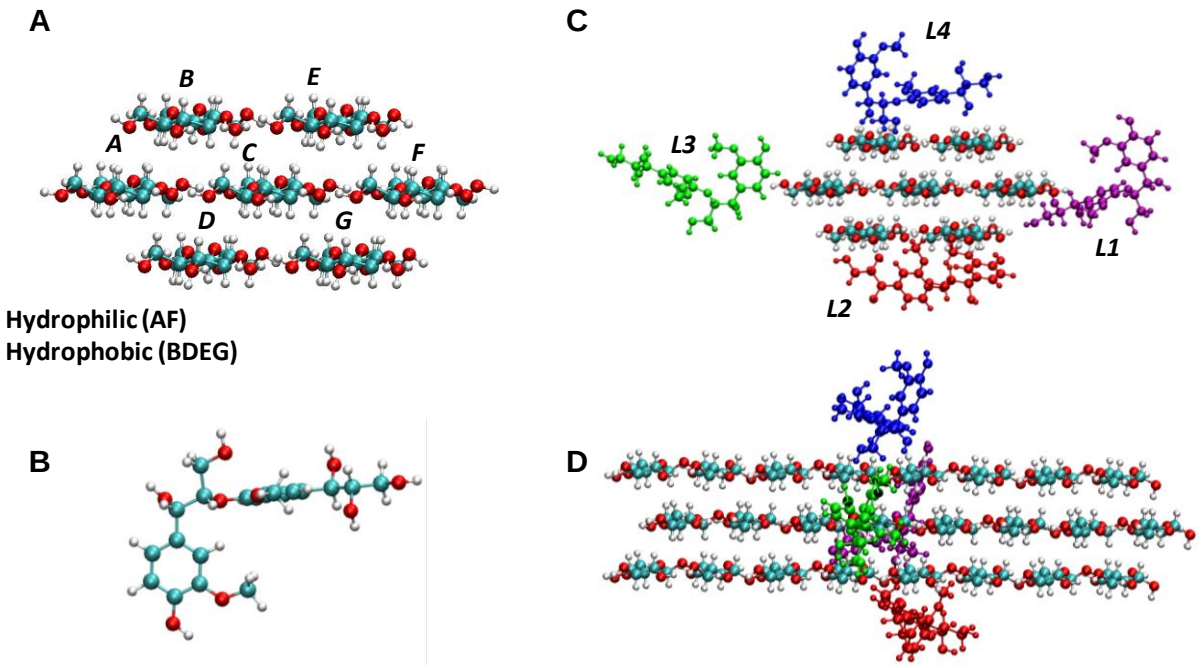

Figure 2 (A) Cellulose nanocrystal model with 7 chains, where the chains BDEG represent the hydrophobic surface, because the less polar aliphatic hydrogen atoms of the glucose rings and the glycosidic bonds are predominantly exposed to the solvent, and the chains AF represent the hydrophilic surface, because the polar hydroxyl groups of the glucose monomers are predominantly exposed to the solvent. (B) Optimized structure in gas phase from quantum-chemistry DFT-PBE calculations of the lignin dimer model. Cellulose-lignin complex front view (C) and side view (D). Lignin dimer color code in the complex is: L1 (purple), L2 (red), L3 (green), and L4 (blue). The color code of the atoms is: oxygen (red), hydrogen (white), and carbon (cyan).

The lignin - cellulose complex was built as follows. Four guaiacyl dimers have been initially placed close to the cellulose surface, at a distance below 3 Å, as illustrated in Figure 2C. This allows us to track lignin adsorption at hydrophilic and hydrophobic sides of cellulose. The lignin-cellulose models were centered in cubic boxes, leaving at least one nm from the longest side of the model to avoid interactions between the lignin-cellulose complexes and their images in the neighboring boxes. We used this rim spacing to determine the size of the box. Each cellulose - lignin system was further solvated with the number of solvent molecules needed to fill the box size, as summarized in the Supporting Information (SI) Table S1. Each organic solvent, i.e. ethanol and acetonitrile, was examined at three different concentrations: pure, 75 wt%, and 50 wt%, and compared with the simulations in pure water. Cellulose-lignin interactions in gas phase have been also studied for comparison.

Molecular Dynamics simulations

All-atom Molecular Dynamics (MD) simulations of each system described in Table S1 were carried out using the GROMACS package 2016.3,[85-89] along with the 4-sites Transferable

Intermolecular Potential (TIP4) for liquid water,[90-92] the CHARMM36 additive force field,[93, 94] and the CHARMM-compatible force field for lignin.[52] The solvent structure for the organic solvents was available at the GROMACS molecule and liquid database.[95]

For each simulation box, energy minimization was performed using the steepest descent algorithm until convergence to a tolerance of 100 $kJ.mol^{-1}.nm^{-1}$. After minimization, restrained simulations were performed for 200 ps at 298.15 K to allow solvent equilibration around the lignocellulosic models. Afterwards, 20-ns MD simulations were performed with a frame-saving rate (for analysis) of 1 ps, in order to study the interaction of the cellulose-lignin complex in the solvent mixtures. To assure that the simulation length would not alter our discussion and conclusions, the error bars of the interaction energies and characteristic torsion angle in cellulose were computed and are reported when relevant (vide infra).

Temperature and pressure coupling were handled using the leap-frog stochastic dynamics integrator and the Parrinello-Rahman method, respectively. Initial velocities were generated from a Maxwell distribution at 298.15 K and the isothermal-isobaric (NPT) ensemble was considered for data collection. Neighbor searching and short-range nonbonded interactions were handled with the Verlet cut-off scheme. Electrostatics were treated with the Fast Smooth Particle-Mesh Ewald method, with a Coulomb cut-off of 1.2 nm, a fourth-order interpolation, and Fourier spacing of 0.12 nm. Van der Waals (vdW) interactions were treated using the Lennard-Jones potential with a cut-off distance of 1.2 nm.

The structures and dynamics were characterized using the incorporated tools within GROMACS. We computed several descriptors to study the interactions between cellulose, lignin, and solvent components. These are: (i) site-to-site radial distribution functions, $g(r)$; (ii) number of hydrogen bonds (H-bonds) and cumulative numbers (cn); (iii) torsion angles of the cellulose backbone and side chains; (iv) solvent-accessible surface areas (SASA),[96] (v) the angle between normal to planes of the lignin phenolic rings, and (vi) torsion angles of cellulose hydroxymethyl chains. Site-to-site $g(r)$ were computed (see Figure 1 for atom numbering) considering the cellulose oxygens as follows: hydroxyl (O2 and O3) and hydroxymethyl (O6), glycosidic bond (O4), and monosaccharide ring (O5)); the lignin oxygens Oα, Oβ, Oγ, and the methoxy groups (OMe); the solvents oxygen atoms in water and ethanol, the nitrogen atom in acetonitrile, and the methyl carbon atoms in ethanol and acetonitrile. The cellulose-lignin $g(r)$ was computed considering carbons of glucose and aromatic ring, respectively. Here, $g(r)$ is normalized by the number of reference points and the volume of the shell. Thus,

$g(r)$ is expressed as number density (atoms/nm^3) per glucose/lignin monomer, and it tends to the bulk density of the particle as *r* increases.

The integration of $g(r)$ from 0 to *r* gives the cumulative number, cn(*r*), of particles within a distance *r* from the cellulose/lignin surface atoms. Here, the cumulative numbers were obtained within a correlation distance of *r*=1.5 nm. H-bonds were calculated using a geometrical criterion with a maximum donor-acceptor distance of 0.35 nm and a donor-hydrogen-acceptor angle of 30°, and they were further normalized by the number of cellulose or lignin monomers. Solvent accessible surfaces were computed using a solvent probe radius of 0.14 nm. The angle between lignin ring planes was evaluated through the angle between the normal of the planes defined by the C1, C3, and C5 (Figure 1B) atoms in each lignin monomer.

Results

Solvent effect on lignin coordination to cellulose

The effect of the considered mono- and bi-component solvents on the coordination of lignin to hydrophilic and hydrophobic sides of cellulose was studied using the model with one cellulose nanocrystal and four lignin dimers (see Figure 2C, D). The cellulose-lignin $g(r)$ in Figure 3A,B reveals that lignin dimers are more coordinated to cellulose in pure water than in mixed solvents, ethanol, or acetonitrile, in agreement with very recent (both experimental and atomistic simulation) observations.[62, 78-81] Thus, our results support the observation that lignin dimers dissociate from cellulose in the presence of the organic cosolvent. Lignin binds cellulose by forming H-bonds as follows from the H-bond probability distribution along the dynamics in Figure 3C,D. The presence of ethanol and acetonitrile decreases the cellulose-lignin coordination significantly, and the effect becomes more notorious in water-organic mixtures, particularly in the water-acetonitrile solvents (Figure 3B). In pure water, the H-bond interactions (H-bond ≥ 1) survived during more than 75% of the simulation time, and the probability to form two H-bonds between cellulose and lignin amounts to ~0.45 (Figure 3C, D black points). In the two pure organic solvents, the formation of cellulose-lignin H-bonds is lower than in water. Lignin forms between 1 and 2 H-bonds with cellulose with a maximum probability of ~0.35 and ~0.30 in ethanol and acetonitrile, respectively. The probability that lignin presents one H-bond with cellulose drops down to the interval 0.26 - 0.19 in 50 and 75 wt% water-ethanol mixtures, respectively (Figure 3C, red and green lines). The decrease of the H-bonding between cellulose and lignin is even stronger in water-acetonitrile binary solvents

(Figure 3D, red and green lines). This evidence a decrease in the electrostatic (H-bonding) interactions between cellulose and lignin upon the addition of the organic ethanol or acetonitrile components in water. Interestingly, the H-bonding recovers partially back in the pure organic solvents (blue lines in Figure 3 C,D).

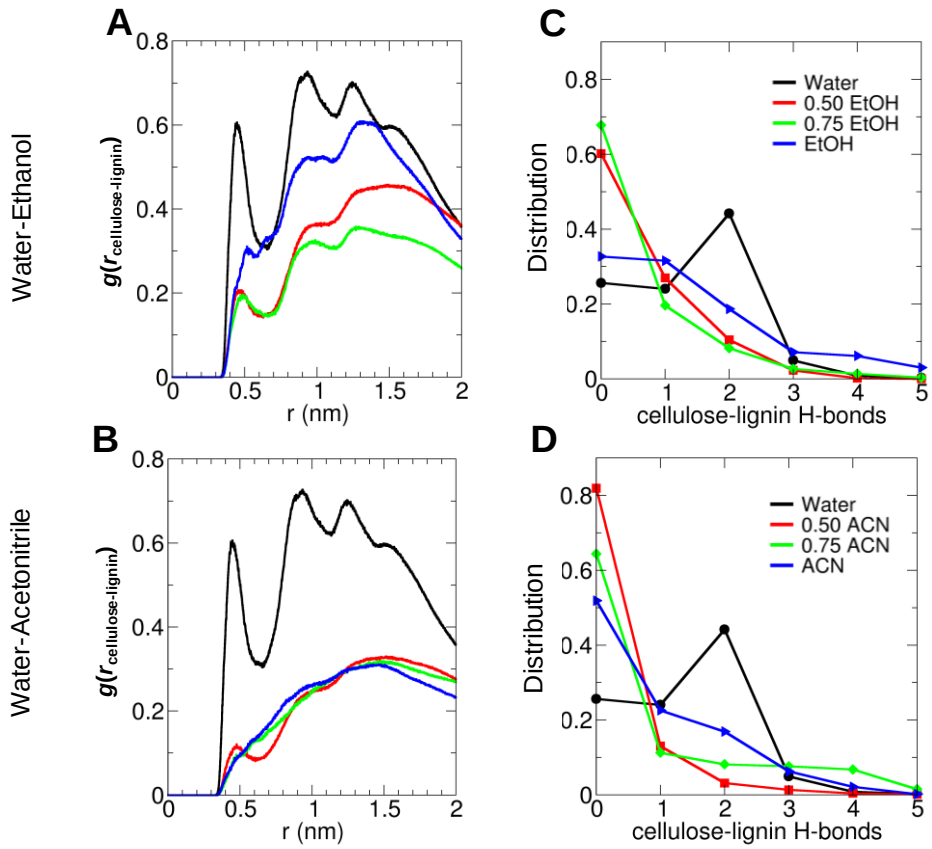

Figure 3. Cellulose-lignin radial distribution function, $g(r)$ in atoms/nm^3, between the surface cellulose monomers and the lignin phenolic rings in (A) water-ethanol and (B) water-acetonitrile solvents; probability distribution of hydrogen bonds between lignin dimers and surface cellulose in (C) water-ethanol and (D) water-acetonitrile solvents. The organic component concentrations are 0, 0.5, 0.75 and 1 mass fraction. H-bond intervals are discrete, but lines have been added to describe better the trends. Scales of the right axes are a guide to the eye.

Accordingly, the average total cellulose-lignin interaction energies in Figure 4 and Table S2 (error bars in Table S2), show the strongest average cellulose-lignin interaction in the presence of water and pure ethanol. From the interaction energy evolution along the dynamics in Figure S1, we infer that cellulose-lignin coordination in water stabilizes after five ns, whereas the interaction in the presence of ethanol decreases slowly. The lignin-cellulose complexation in gas-phase is significantly stronger, as follows from the interaction energies, also reported for comparison in Tables S2. Furthermore, the lignin dimers L2 and L4 (see Figure 2 for notation)

in contact with the hydrophobic chains BD and EG, respectively, display on average stronger interaction energies with cellulose than the lignin dimers L1 and L3, which were initially placed closer to the most hydrophilic chains. The average interaction energies of L1 and L3 with cellulose is in the order of only a few kJ/mol (see Table S3).

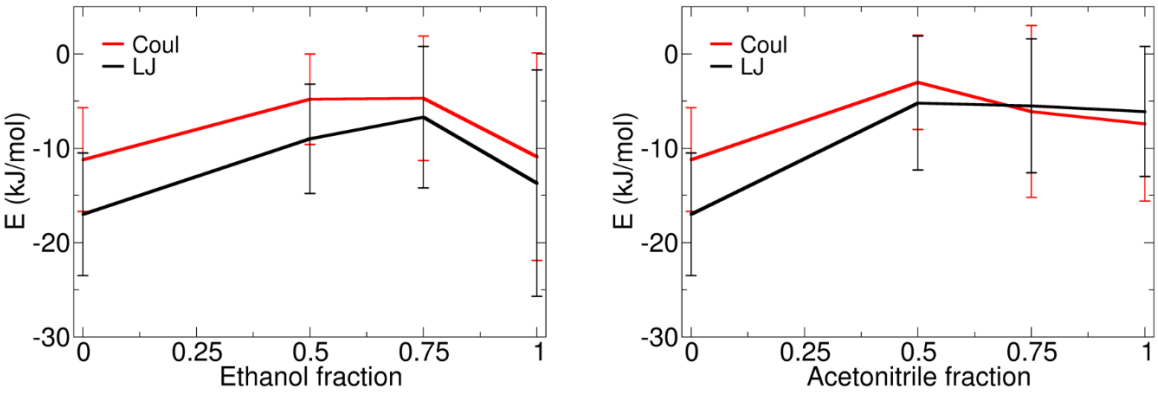

Figure 4. Average lignin-cellulose intermolecular Lenard-Jones (LJ) and Coulomb (Coul) energies per lignin dimer, in pure and ethanol (left), and acetonitrile (right) binary aqueous solvents.

During the dynamics simulation, L1 and L3 disassemble rapidly from cellulose in water, which is in agreement with previous works showing that lignin molecules preferentially aggregate into the hydrophobic faces of crystalline cellulose fibers.[58, 62] The preferential interaction of L2 and L4 with the hydrophobic cellulose surfaces, where the less polar aliphatic hydrogen atoms of the glucose rings are exposed (chains BDEG), shows that vdW interactions play a stabilizing role in the mechanism of adsorption of lignin to cellulose[48] in addition to the H-bond electrostatic interactions.

The most-favored energetical interactions correspond to stable structures of the lignin-cellulose complexes, as displayed in Figure 5. Aromatic rings of lignin adopt a preferential parallel orientation relative to the cellulose surface in water (Figure 5A), as already established previously.[48, 49] The electrostatic interactions between the alcohol groups (i.e. OαH and OγH) of lignin and the hydroxyls of cellulose are favored. Lignin acts as an H-bond donor,[48] and the $O\alpha_{lignin}$ - H… $O3_{cellulose}$ and $O\gamma_{lignin}$-H…$O2_{cellulose}$ H-bonds are formed. These O…O distances are within ~0.25 – 0.30 nm as indicated by the $O\alpha_{lignin}$-$O3_{cellulose}$ and $O\gamma_{lignin}$-$O2_{cellulose}$ sharp pics of $g(r)$ in Figs 5A, right panels.

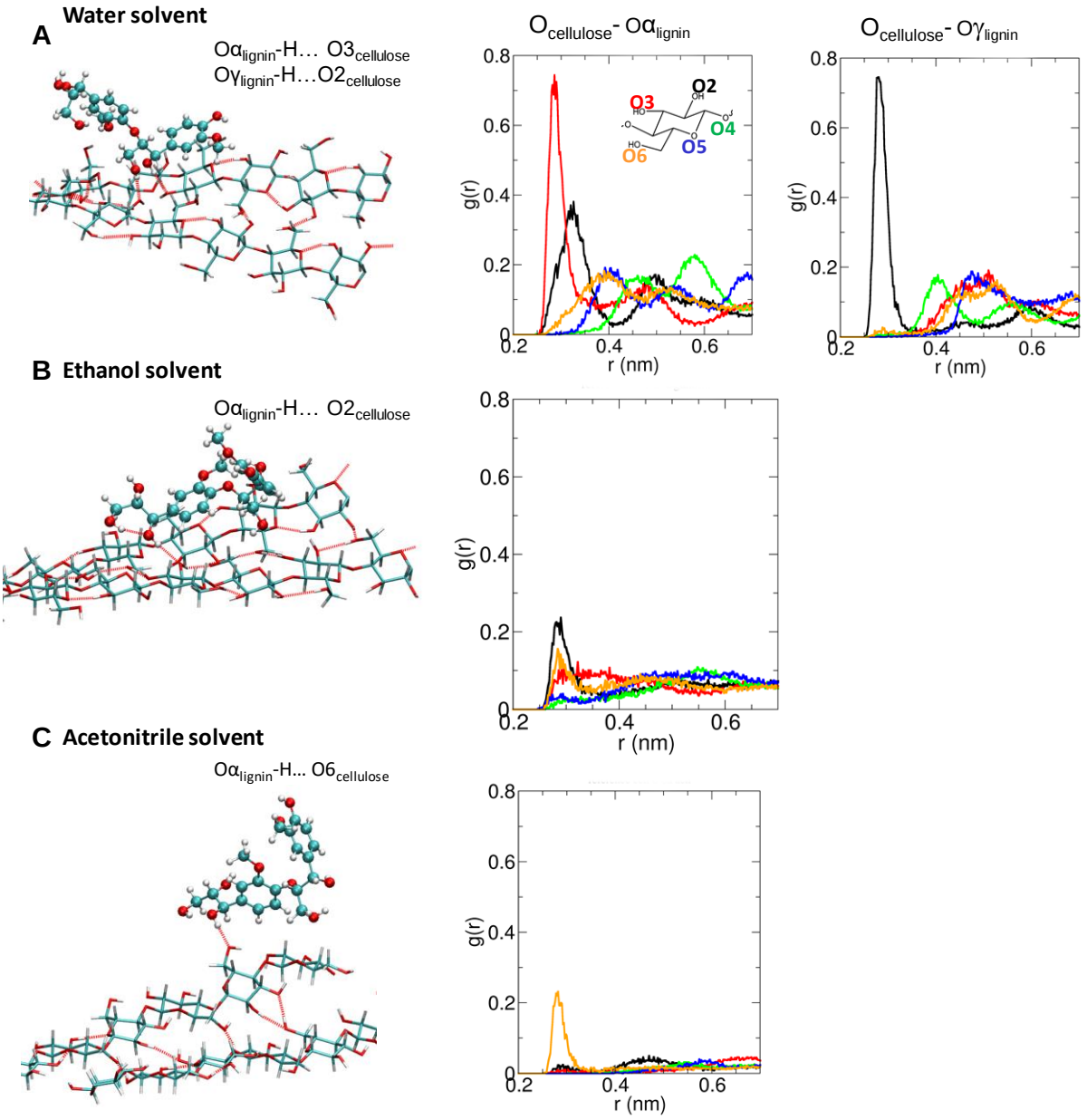

Figure 5. MD snapshots (left panels) of most stable cellulose-lignin complexes and the radial distribution functions ($g(r)$ in atoms/nm^3) (center and right panels) to illustrate the mostly coordinated $O_{lignin}…O_{cellulose}$ pairs in water (A), ethanol (B), and acetonitrile (C) solvents. In the MD snapshots solvents are not shown for clarity and H-bonds are shown with red dashed lines. Only $g(r)$ of lignin-cellulose H-bonds are shown next to the molecular structure to indicate the most stable configuration. The complete set of $g(r)$of lignin-cellulose can be found in Figs S2-S4. Scales of the right axes are a guide to the eye.

In ethanol (Figure 5B), the H-bond between Oα of lignin and $O2_{cellulose}$ prevails, whereas in acetonitrile (Figure 5C) a significantly less stacking between lignin aromatic ring and cellulose glucose is observed despite the probability to form H-bond with O…O distance of ~0.3 nm between lignin Oα and $O6_{cellulose}$ as indicated by $g(r)$ in Figure 5C, right panel.

In the mixed solvents, the lignin coordination to cellulose is disrupted. In accordance with the minimum lignin-cellulose interaction energies (Figure 4 and Tables S2, S3), the radial distribution functions of the six oxygen sites in cellulose surfaces and the three O_{lignin} atoms (O_α, O_γ, and OMe) in Figs S2 – S4 reveal no well distinguishable contacts between lignin and cellulose oxygens along the dynamics. The stacking interactions between the surface cellulose monomers and the lignin phenolic rings are also negligible in the binary aqueous solvents, according to $g(r)$ in Figure 3. It appears that water and organic molecules in the binary solvent mixtures act together to disrupt the lignin adsorption on cellulose. This leads to the hypothesis that preferential interactions between cellulose or lignin with each component of the water-organic solvent have an effect on the lignin adsorption on cellulose.

Preferential interactions between solvents and cellulose – lignin complex

The organization of solvent molecules around O2, O3, O4, O5, and O6 sites in cellulose are identified from the $O_{cellulose}$-$X_{solvent}$ ($X_{solvent}$ = O_{water}, $O_{EtOH,}$ and N_{ACN}) radial distribution functions $g(r_{Ocellulose\text{-}Xsolvent})$, while distinguishing between the hydrophilic AF and hydrophobic BDEG chains. A well-structured water layer forms around both hydrophilic and hydrophobic surfaces in agreement with previous cellulose-water studies [32], mainly because of water structuring around O6, O2, and O3 sites. This follows from the sharp peaks (Figure 6 A,B) in O6, O2, and O3 $g(r_{Ocellulose\text{-}OWater})$ profiles at ~0.28 nm and a minimum of the first coordination shell near 0.35 nm. The coordination order is O6>O2>03. The other two oxygen sites (O4 and O5) do not display well-defined coordination to water. In the pure ethanol solvent, the same O6, O2, and O3 cellulose sites coordinate preferably to ethanol molecules, as concluded from the sharp peaks in $g(r_{Ocellulose\text{-}OEtOH})$ at ~0.29 nm and their minima of the first coordination shells between ~0.36-0.37 nm in Figure 6 C,D. Ethanol, similar to water, shows a slight preferential coordination to the hydrophilic AF cellulose surface. At the hydrophobic surface (chains BDEG), the peak intensity is decreased and O6 coordination is reduced to the coordination of O2. Note that the number density between O_{cell} and O_{EtOH} decreases (lower $g(r_{Ocellulose\text{-}OEtOH})$intensity) in comparison with those with $O_{water,}$ as expected from the larger ethanol molecular size. In acetonitrile solvent, $g(r_{Ocell\text{-}NACN})$ profiles in Figure 6 E,F indicate that only cellulose oxygens O2 and O6 coordinate to N_{ACN} below 0.35 nm, at ~0.29 - 0.30 nm. The acetonitrile molecules coordinate predominantly to O2 with a preference for the hydrophobic cellulose surfaces (see Fig 6C).

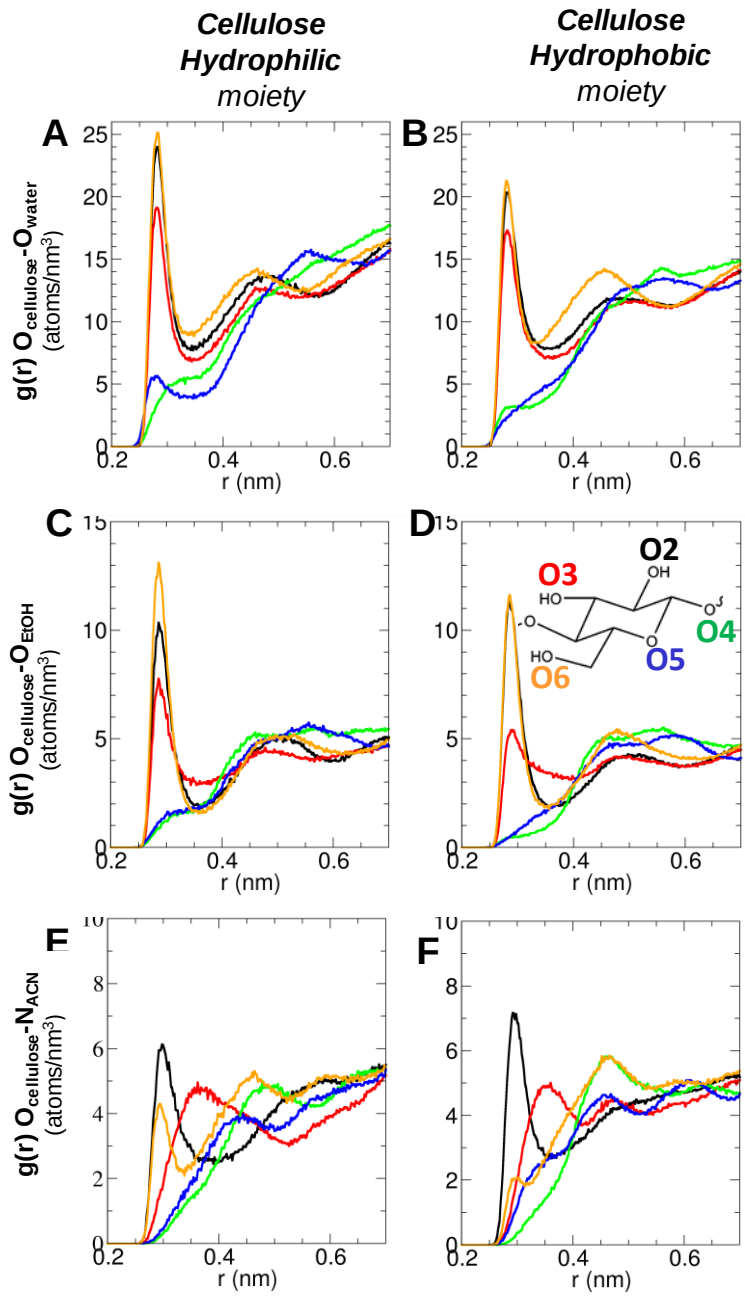

Figure 6. Radial distribution functions, ($g(r)$ in atoms/nm^3) of the $O_{cellulose}$-$X_{solvent}$ pairs in pure (A, B) water, (C, D) ethanol, and (E, F) acetonitrile solvent, in chains AF (hydrophilic cellulose moiety) and chains BDEG (hydrophobic cellulose moieties). $O_{cellulose}$ color code is O2 (black), O3 (red), O4 (green), O5 (blue), and O6 (orange), see Figure 1 for oxygen notation. The solvent reference site X denotes, respectively, the oxygen atom in water and ethanol (EtOH), and the nitrogen atom in acetonitrile (ACN). Scales of the right axes are a guide to the eye.

The mono-component solvent molecules do not compete strongly with lignin for the same oxygen site in cellulose, i.e. water and ethanol preferably coordinate O6-cellulose, whereas lignin–cellulose most probable H-bonds are with O2 and O3 cellulose sites (see Figure 5A,B). Similarly, acetonitrile–cellulose preferential binding site is O2 and lignin-

cellulose complex in acetonitrile solvent is stabilized via O6…Oα_{lignin} H-bond (Figure 5C).

The addition of the organic solvent fraction into water does not, in overall, alter the solvent-cellulose preferred coordination trends obtained for their mono-component counterparts as found from $g(r)$ in Figure S5, S6. An exception is a preferred coordination of ethanol to O2 instead of O6 at the hydrophobic cellulose sites, i.e. O2>O6>03. This change of ethanol preference is most likely due to the presence of water, which competes with ethanol for the same coordination sites.

The number of water molecules in the first solvation shell decreases with the organic cosolvent concentration, as indicated by the computed cumulative number, cn(r), plotted in Figure 7 for an extended range of cosolvent concentration, including also 25wt% cosolvent in water. As a general trend, the water number density is expected to decrease with the addition of a larger organic solvent. This is observed only below 50 wt% concentrations of both ethanol and acetonitrile, where cn(r) corresponding to water/cosolvent only linearly decreases/increases. This effect is, however, not homogeneous in 50-100 wt% cosolvents concentrations: it is instead modulated by the nature of the cosolvent and the properties of the cellulose surfaces. As follows from Figure 7A, significantly more water molecules are displaced by acetonitrile than by ethanol from the solvation shell on the hydrophobic cellulose surface. Acetonitrile molecules accumulate preferably at the hydrophobic cellulose sites, whereas the ethanol molecules accumulate equally at the AF and BDFG chains (Figure 7B). Thus, acetonitrile has a rather hydrophobic character as lignin, and ethanol an amphiphilic character. The stronger water exclusion by acetonitrile can be explained by the coordination of the hydroxymethyl group of cellulose to the methyl group of acetonitrile (see $O_{cellulose}$-CMe $g(r)$ in Figure S6.). This is most likely because of dipole-dipole interactions between acetonitrile molecules, which displace methyl groups toward the cellulose surface and form $O_{cellulose}$…H-CMe bonds. Moreover, the local microheterogeneity of water-acetonitrile mixtures[97] could enhance the water-acetonitrile separation when in contact with the different cellulose surfaces as exemplified in Figure 7B,C. Ethanol and water, on the contrary, remain less separated, as ethanol-water mixtures are more homogeneous and both components share a similar affinity for a specific oxygen site in cellulose.

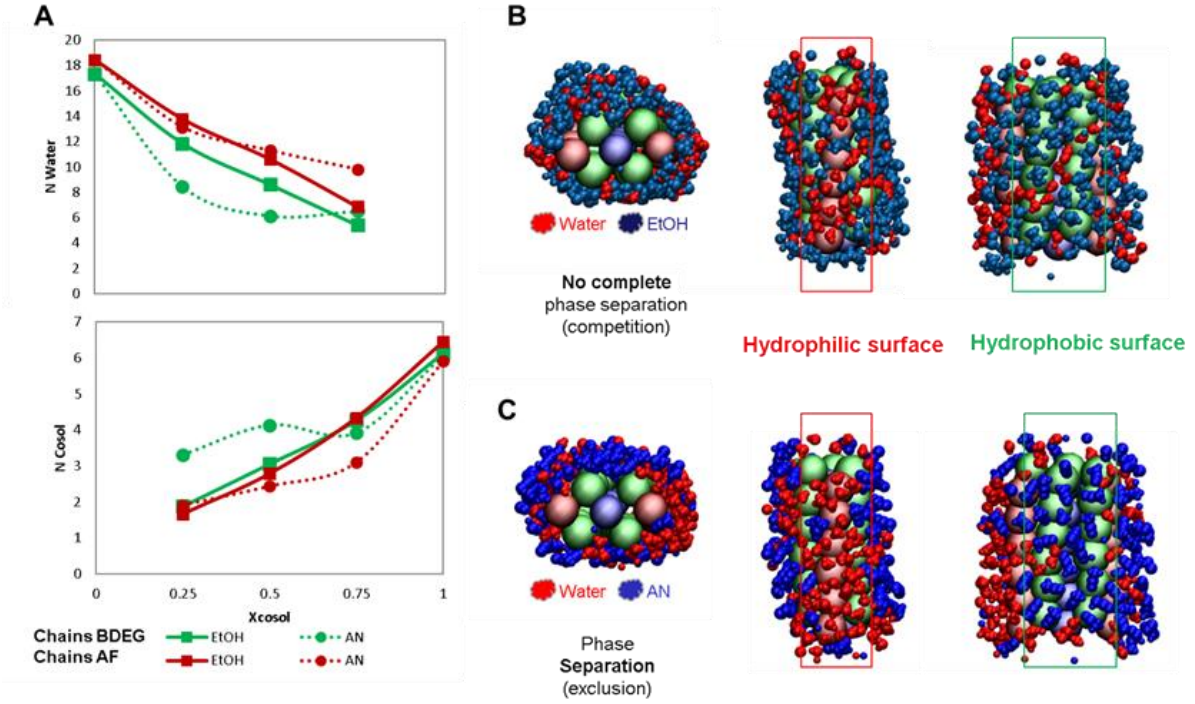

Figure 7. (A) Cumulative number of molecules of water (N Water, top) and organic cosolvent (N Cosol, bottom) within 0.7 nm from the cellulose glycosidic oxygen as a function of organic solvent concentration (X_{cosol}). Circles denote acetonitrile (AN) and squares denote ethanol (EtOH) cosolvents. (B) Snapshots illustrating 0.5 nm solvation shell around cellulose surfaces in 75 wt% ethanol (B) and 75 wt% acetonitrile (C) mixtures. Pink and green beads represent glucose monomers on, respectively, hydrophilic and hydrophobic surfaces of cellulose; water and cosolvents are represented by red and blue vdW surfaces, respectively.

The interaction between solvent components and lignin has been studied from the computed radial distribution functions $g(r_{\text{Olignin-Xsolv}})$ between lignin oxygens (Oα, Oγ, OMe, and O4) and X_{solv} sites: O_{OH} and C_{Me} in ethanol, O in water, and N, and C_{Me} atoms in acetonitrile. The $g(r_{\text{Olignin-Xsolv}})$results for the pure solvents in Figure 8 reveal well-structured solvation layers around Oα and Oγ in lignin dimers, whereas Oβ and OMe are significantly less coordinated. Water (Figure 8A) and ethanol (Figure 8 B,C) oxygen atoms display the highest number density when coordinated to Oα and Oγ, whereas acetonitrile coordination is significantly less structured (Figure 8 D,E). On the other hand, it follows from $g(r_{\text{Olignin-}C_{ACN}})$ that acetonitrile methyl carbons are well structured in the first solvation shell, interacting through the aliphatic hydrogens with the lignin alcohol groups. Thus, acetonitrile displays a head (N, H-bond acceptor) and tail (methyl) interaction with lignin (as with cellulose), whereas ethanol shows predominantly a head-type (O, H-bond acceptor/donor) interaction.

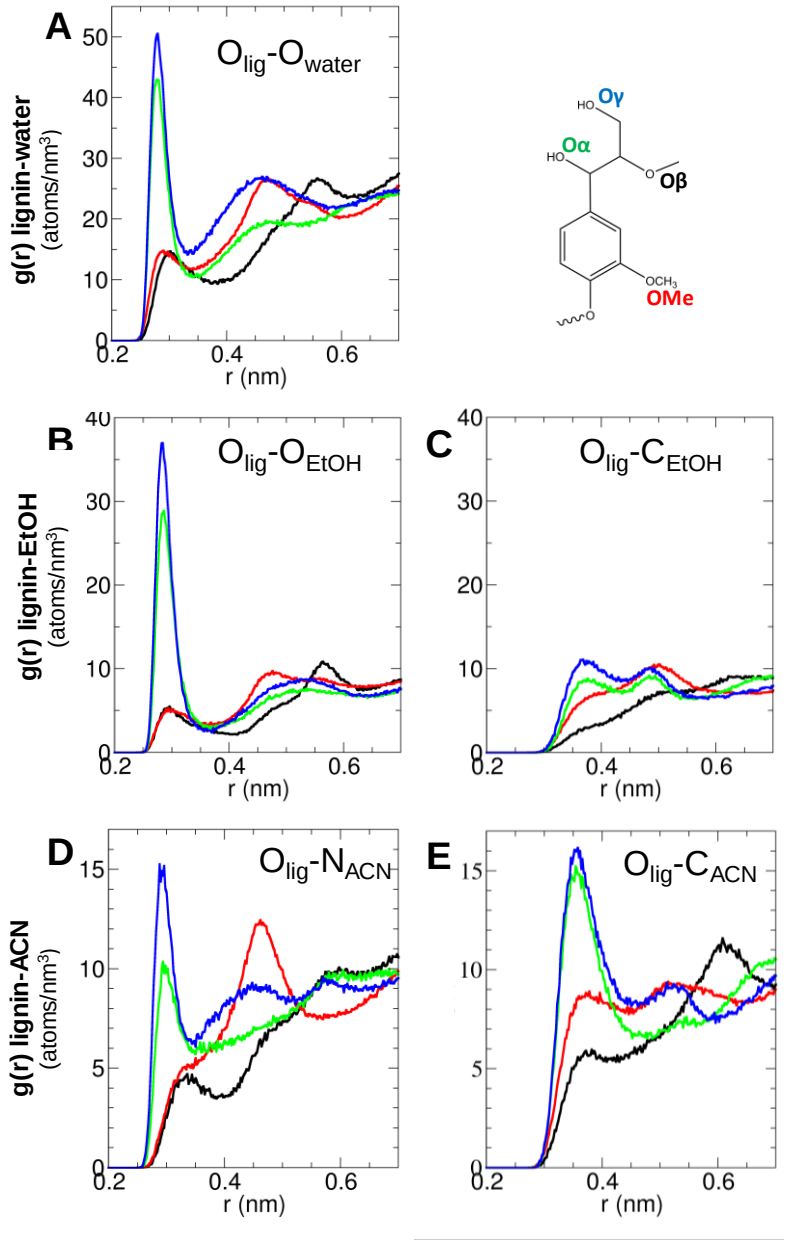

Figure 8. Radial distribution functions, ($g(r)$ of the Olig.-Xsolv pairs, Xsolv = O in water (A) and ethanol, EtOH (B) , Xsolv = C(CH_3) in ethanol (C), Xsolv = N and C(CH_3) in acetonitrile, ACN (D, E). O_{lig} color code is OMe (red), Oβ (black), Oα (green), and Oγ (blue). Scales of the right axes are a guide to the eye.

Solvent induced conformational changes of cellulose and lignin

Another reason leading to the detachment of lignin dimers from cellulose could be solvent-induced conformational changes, which may decrease the number of accessible sites in cellulose and lignin and disrupt their coordination. First, we measured the glycosidic torsion angle Φ (O5-C1-O4′-C4′) in cellulose, which describes the relative orientation of adjacent glycosyl residues in the same chain.[2] The maximum of the probability distributions of the

glycosidic torsion angle Φ (not shown) falls near ~-88° in water, whereas narrower distributions profiles (by 1-2°) are found for the pure organic and mixed water-organic solvents. These distributions are shifted by 10° in comparison to the Φ value for the crystal-like cellulose (-98.7°), and describe a twisting of the chain's backbone, as reported in previous MD simulations of cellulose.[34-37, 39, 40] The chirality amplification in MD simulations of finite length crystals with explicit chain ends can result in a twist along the cellulose chain axis,[36] which is most likely promoted by surface-mediated conformational changes of the hydroxymethyl group.[35]

It is expected that this twisting has an effect on the solvent-accessible surface area (SASA) of cellulose. However, the backbone access to the solvent is limited. We, therefore, focused on the solvent-induced changes of hydroxymethyl torsion angle ω (O5-C5-C6-O6)[2] (illustrated in Figure 1). Three low-energy conformations are possible: ω = tg, gt, and gg, referring to the gauche or trans positions of O6 relative to both O5 and C4 in cellulose. Ideal tg, gt, and gg conformations are characterized by ω = 180°, 60°, and -60°, respectively.[2, 98, 99] In the tg and gt conformations, the position of the C6-O6 bond is equatorial with respect to the glucose ring; in the gg conformation, the C6-O6 bond is axial (see Figure 1). In the bulk crystalline cellulose Iβ,[2, 83] the hydroxymethyl groups adopt the tg conformation, with an average value of ω =169.4°, and participate in an intramolecular H-bond with the adjacent glucose monomer (O2-H…O6'), at the expense of intermolecular H-bonds.

For the analysis of ω, we used the gg-gt-gg occurrence frequency, which was computed in angle intervals define as following: gg=(-120, 0), gt=(0, 120), and tg=(±180, ±120) for the hydrophilic AF (Figure 9A) and the hydrophobic BDEG (Figure 9B) chains. The convergence of the torsion angles during the MD simulations was verified using the averaged block analysis of ω (O5-C5-C6-O6) reported in Table S4 and of the root mean square displacement (RMSD) of the positions of cellulose hydroxymethyl groups atoms in Table S5.

In pure water, the gg conformers prevail at AF chains (nearly 70 wt%), whereas at BDEG, the gg conformers are only ~10 wt%. This is consistent with the hydrophilic/hydrophobic character of the respective cellulose chains. The increase of ethanol/acetonitrile component in water causes transitions from gg to gt or tg in AF chains, as follows from the decrease of the occurrence of the gg conformers in Figure 9A.

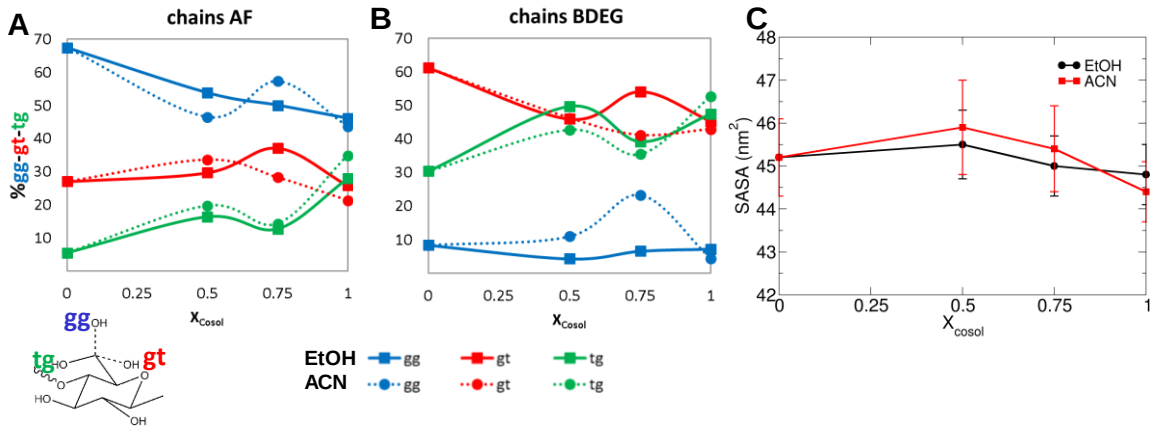

Figure 9. (A) and (B): hydroxymethyl dihedral (% gg-gt-tg) of cellulose in pure and mixed solvents. Color code: gg (blue), gt (red), tg (green). The symbols used for the different solvents are: ethanol (square, full line); acetonitrile (circle, pointed line). (C): solvent accessible surface area (SASA) of cellulose.

The gg conformers, however, remain the majority in the mixed and pure organic solvents, indicating a predominant hydrophilic character of AF chains. Interestingly, the organic solvent component in water leads to a slight increase of the hydroxymethyl gg conformers in BDEG chains, thus decreasing their hydrophobicity. This is most pronounced in 75 wt% acetonitrile-water mixture, where the presence of gg-conformers is doubled. A gt→tg transition occurs at the hydrophobic BDEG surface with the increase of the ethanol/acetonitrile component towards the pure organic solvents. This indicates an improved intramolecular H-bonding in cellulose (vide supra), as the number of intramolecular cellulose H-bonds is better preserved in the pure organic solvent than in water.[64] Albeit this effect of organic co-solvents modifies the accessibility of different surface oxygens, it scantily affects the geometrical SASA of cellulose, as shown in Figure 9C.

The effects of the lignin conformations in different solvents were described by the evolution of the SASA of lignin dimers (Figure 10A), the ring-ring distance between the phenolic rings (d_{CoM} in Figure 10B), and the angle between the planes of these rings (α in Figure 10C). In water, a bad solvent for lignin, the lignin dimer has the smallest average SASA, which is, however, broader than the lignin SASA of a single lignin dimer in water.[64] This reveals that cellulose stabilizes lignin in the adsorbed state by reducing its hydrophobic interactions with the water solvent. In comparison with the mixed and pure organic surfaces, the lignin interactions with water are the least favorable.

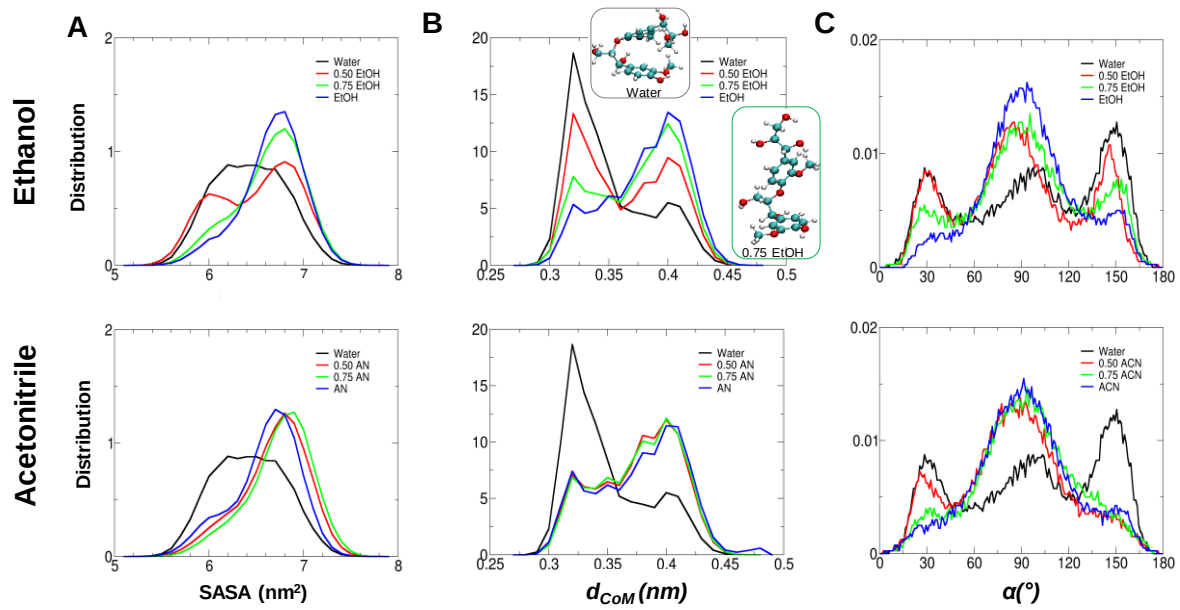

Figure 10. (A) Average distributions of solvent accessible surface area, SASA, of lignin dimer; (B) average center-of-mass ring-ring distance distribution of guaiacyl monomers in the lignin dimer, (C) average angle distribution between ring planes of lignin models, at different ethanol concentration. (D-F) idem as (A-C), respectively, at different acetonitrile concentrations. The insets in the upper panel of (B) show the lignin dimer conformers from the cluster analysis in water and 0.75 wt% EtOH-water solvents.

The most stacked lignin conformation is found in water with the shortest ring-ring distance of 0.32 nm and α ~150° (Figs. 10B,C). In the mixed solvents, where the lignin is detached from cellulose, SASA increases, which reveals more favorable interactions of lignin dimer with the mixed aqueous solvents than with water alone. As a consequence, lignin adopts rather a T-shaped staked conformation with the ring-ring distance of ~0.4 nm and α equal to 90°. In the pure organic solvents, the cellulose-lignin coordination is partially recovered; however, SASA of lignin decreases only slightly. These results, although obtained for a limited lignin size model, agree reasonably well with the results of Smith et al.,[72] reporting that lignin polymers with up to 60 units in water-tetrahydrofuran (THF) mixtures adopt an unfolded conformation with increased SASA, whereas, in pure water, lignin polymers adopt a crumbled globular-like shape, with a considerably reduced SASA. Moreover, a recent study of lignin solubility in water-ethanol mixtures has identified maximum solubilization at 60 wt% ethanol[100] which is expected to result in more extended conformations of lignin polymers.

Correlation between solvents preferential interactions, conformational changes, and cellulose-lignin coordination

The cellulose-lignin interaction energies and their evolution along dynamics simulations demonstrate that the introduction of the organic solvents in water results in a substantial disruption of cellulose-lignin interactions. The addition of the organic phase (ethanol/acetonitrile) modifies predominantly the cellulose solvation shells resulting in reduced mobility of water molecules because of the longer-lasting cellulose-water H-bonds (in Table S6), concomitant with the longer-lasting water-ethanol and water-acetonitrile H-bonds than the water-water H-bonds in the bulk water.[97] In addition to the effect on the water mobility, the organic phases compete with water for the same cellulose coordination site, which interferes with the lignin adsorption on cellulose. In pure water, the strong $O6_{celllulose}$-O_{water} coordination governs the lignin interaction towards O3 and O2 of cellulose, as follows from $O_{cellulose}$-O_{lignin} $g(r)$ in Figure 3. Ethanol competes with water for the same cellulose oxygen sites and its mixture with water effectively disrupts, $O3_{cellulose}$-$O\alpha_{lignin}$ and $O2_{cellulose}$-$O\gamma_{lignin}$ H-bonds with increasing ethanol concentration from 50 to 75 wt%. The presence of water favors ethanol coordination to $O2_{cellulose}$ in the hydrophobic DBEG chains and $g(O_{cell}$-$O_{EtOH})$ follows the order O2>O6>03 (Figure S5 B). This limits the lignin coordination to O2 sites, which, in our model, results in a complete disruption of lignin-cellulose coordination. The number of ethanol molecules coordinated to the hydrophobic cellulose chains attains its maximum at 75 wt% ethanol concentration, the cosolvent concentration at which the cellulose-lignin interaction energy has minimal value (see Figure 4). In the 100 wt% ethanol solvent, lignin recovers back the $O2_{cellulose}$-$O\gamma_{lignin}$ H-bond.

Contrary to ethanol, N atoms in acetonitrile do not compete with water for the same cellulose oxygen sites. As a result, the preferred N coordination to O2 and O3 cellulose atoms is preserved up to the largest extent in 50, 75, and 100 wt% co-solvent concentrations, and this is particularly true for the acetonitrile coordination to BDEG chains (Figs. 6E,F and S6B), at which lignin adsorbs predominantly. Acetonitrile, however, competes with water for O6 in cellulose with its methyl group carbons and builds a solvation shell around cellulose O6 sites (see $g(O_{cellulose} - C_{ACN})$ in Figure S8 C,D) via C-H…O6 bonds. Mixing water with acetonitrile, therefore, enhances the coordination of both solvent components around cellulose and hinders more effectively the accessibility of lignin to its preferred oxygen centers (O2, O3, and O6).

This results in a disruption of cellulose-lignin attachment in 50 and 75 wt% acetonitrile-water mixtures. On the other hand, acetonitrile tends to exclude water from the coordination shell of the hydrophobic BDEG chains, which is expected to diminish the notorious effect of acetonitrile-water competition for O6 in cellulose. This exclusion is more efficient with increasing acetonitrile concentration from 50 to 75 wt % in its aqueous mixtures, which might explain the improved stabilization of the lignin-cellulose complex at 75 wt% acetonitrile-water solvent (see lignin-cellulose interaction energies in Figure 4). Finally, the lack of water in 100 wt% acetonitrile enhances the cellulose-lignin binding via $O\alpha_{lignin}$-H…$O6_{cellulose}$.

The solvent-induced conformational changes from *gt* to *tg* at BDEG moieties favor the cellulose intra-chain H-bonds and, additionally, decrease the probabilities of lignin to cellulose H-bonding. The excess of *tg* conformers in the pure organic solvents contributes to the weaker lignin-cellulose binding in comparison to that in pure water.

The preferred coordination of the solvent components to lignin seems to be less efficient in disrupting lignin adsorption on cellulose. The first solvation shells of the three solvent components are well-defined around the lignin Oα and Oγ in both pure and binary mixtures. The solvent components preserve their coordination order to Oα and Oγ in the mixtures, except acetonitrile, which displays a higher preference for the Oα site than Oγ coordination in the 50 wt% aqueous binary solvent. This could additionally contribute to disrupting more effectively $O\alpha_{lignin}$-H…$O6_{cellulose}$.

Finally, analyzing the interaction energies of lignin or cellulose with the solvents, we found that the interactions with water are typically electrostatically driven (Figs. S9, S10; left panels). The cellulose-lignin interactions with ethanol have significantly stronger vdW contributions (Figure S9, right panel) in water-ethanol mixtures. In the water-acetonitrile and pure acetonitrile solvents, the vdW forces dominate, as evidenced by the stronger vdW energies in Figure S10, right panel. Thus, when compared with the $O_{cellulose}$-$X_{solvent}$ preferential coordination, the coordination of O6 sites in cellulose to water and ethanol molecules is mostly electrostatically driven, whereas coordination of acetonitrile to the less exposed O2 or O3 sites is rather driven by vdW forces.

Conclusions

The adhesion of lignin to cellulose in the presence of a mixed solvent does not depend only on variations of solubility of lignin with the composition of the solvent. The competition of each

solvent component for specific sites on lignin and cellulose modifies the availability of adsorption sites and the energetics of the allowed interactions. Molecular dynamics simulations are the proper tool to describe the atomistic-level coordination of lignin to cellulose. Computation of radial distribution functions $g(r)$ and analysis of hydrogen bonds allows evaluating the effect of ethanol and acetonitrile -examples of solvents with different polarities- in a binary mixture with water on the interactions between cellulose and lignin. The conformations of these biomass components in different solvents can also be determined and plays a significant role in the adhesion phenomena.

When pure solvents are considered, water is the medium that mostly favors the adsorption of lignin on cellulose, followed by ethanol and acetonitrile. In the mixed solvents, the cellulose-lignin interaction is strongly disrupted. In the binary mixtures, the specific organization of each co-solvent component around the cellulose is the most important factor affecting the geometries and the energetic stability of the cellulose-lignin complex. The competition between ethanol and water for the same oxygen sites of cellulose leads to a more effective disruption of the cellulose-lignin complex at increasing ethanol concentration. Acetonitrile methyl carbon coordinates to O6 in cellulose, the preferred site for water coordination. This competition, similarly to ethanol-water, favors lignin detachment from cellulose. At the same time, acetonitrile tends to segregate on the hydrophobic cellulose chains, excluding water molecules. This effect is highly non-linear. The more efficient exclusion of water at 75 wt% acetonitrile concentration decreases the role of acetonitrile-water competition and allows a better stabilization of cellulose-lignin complex than in 50 wt% acetonitrile co-solvent. The obtained non-linear behavior of cellulose-lignin coordination strengths with the increase of the ethanol content is in qualitative agreement with recent experimental findings on the solubility of lignin in water-ethanol mixtures.[100]

In the absence of water, lignin-cellulose coordination recovers partially. The weaker interactions between lignin and cellulose in pure organic solvents than in pure water correspond to the ethanol/acetonitrile-induced conformational changes in cellulose hydroxymethyl groups *gt -> tg,* which favor the intra-chain H-bonds in cellulose and decrease the availability of lignin adsorption sites.

The higher effectiveness of mixed water-organic solvents for the fractionation of biomass by organosolv treatments has often been observed. Better solubilization of the lignin fragments has been generally considered as the main role played by the organic solvent component. Our

results suggest that the effect of mixed solvents on adhesion and separation is a more complex interplay between components of the solvent and different fractions of biomass.

Supporting Information. Configuration and sizes of the simulated systems. Average energies (with the error bars) of lignin-cellulose interactions**.** Average block analysis of the torsion angle ω (O5-C5-C6-O6) in cellulose chains. Average block analysis for RMSD of the positions of atoms in cellulose hydroxymethyl groups. H-bond lifetimes for the cellulose-water and cellulose-cosolvent interaction types. Radial distribution functions and solvent-cellulose, and solvent-lignin interaction energies.

Acknowledgments

This work was partially funded by an ENSCM PhD grant in the framework of the SINCHEM Joint Doctorate program under the Erasmus Mundus Action 1 Programme (FPA 2013-0037). Access to the HPC resources of CCRT/CINES/IDRIS was granted under the allocation A0070807369 by GENCI.

REFERENCES

(1) Ragauskas, A.J.; Williams, C.K.; Davison, B.H.; Britovsek, G.; Cairney, J.; Eckert, C.A.; Frederick, W.J.; Hallett, J.P.; Leak, D.J.; Liotta, C.L.; Mielenz, J.R.; Murphy, R.; Templer, R., and Tschaplinski, T., The Path Forward for Biofuels and Biomaterials. *Science* **2006**, *311*, 484-489.

(2) Nishiyama, Y.; Langan, P., and Chanzy, H., Crystal Structure and Hydrogen-Bonding System in Cellulose Iβ from Synchrotron X-ray and Neutron Fiber Diffraction. *J. Am. Chem. Soc.* **2002,** *124*, 9074-9082.

(3) Sun, J.X.; Sun, X.F.; Zhao, H., and Sun, R.C., Isolation and characterization of cellulose from sugarcane bagasse. *Polym. Degrad. Stab.* **2004**, *84*, 331-339.

(4) Fernandes, A.N.; Thomas, L.H.; Altaner, C.M.; Callow, P.; Forsyth, V.T.; Apperley, D.C.; Kennedy, C.J., and Jarvis, M.C., Nanostructure of cellulose microfibrils in spruce wood. *Proc. Natl. Acad. Sci. U.S.A.* **2011**, *108*, E1195-E1203.

(5) Parham, R.A. and Gray, R.L., Formation and Structure of Wood, in *The Chemistry of Solid Wood*. **1984** American Chemical Society. p. 3-56.

(6) Winandy, J.E. and Rowell, R.M., Chemistry of wood strength, in *Handbook of wood chemistry and wood composites*, C. Press, Editor. **2005**: Boca Raton, Fla.

(7) Yamamoto, H.; Ruelle, J.; Arakawa, Y.; Yoshida, M.; Clair, B., and Gril, J., Origin of the characteristic hygro-mechanical properties of the gelatinous layer in tension wood from Kunugi oak (Quercus acutissima). *Wood Sci. Technol.* **2010**, *44*, 149-163.

(8) Besombes, S. and Mazeau, K., Molecular dynamics simulations of a guaiacyl β-O-4 lignin model compound: Examination of intramolecular hydrogen bonding and conformational flexibility. *Biopolymers* **2004**, *73*, 301-315.

(9) Nations, F.a.A.O.o.t.U., *Forest Products Yearbook 2016*. **2018**: Roma.

(10) Zakzeski, J.; Bruijnincx, P.C.A.; Jongerius, A.L., and Weckhuysen, B.M., The Catalytic Valorization of Lignin for the Production of Renewable Chemicals. *Chem. Rev.* **2010**, *110*, 3552-3599.
(11) Doherty, W.O.S.; Mousavioun, P., and Fellows, C.M., Value-adding to cellulosic ethanol: Lignin polymers. *Ind. Crops. Prod.* **2011**, 33, 259-276.
(12) Rinaldi, R.; Jastrzebski, R.; Clough, M.T.; Ralph, J.; Kennema, M.; Bruijnincx, P.C.A., and Weckhuysen, B.M., Paving the Way for Lignin Valorisation: Recent Advances in Bioengineering, Biorefining and Catalysis. *Angew. Chem. Int. Ed.* **2016**. *55*, 8164-8215.
(13) Rinaldi, R., A Tandem for Lignin-First Biorefinery. *Joule* **2017**, *1*, 427-428.
(14) Li, M.-F.; Yang, S., and Sun, R.-C., Recent advances in alcohol and organic acid fractionation of lignocellulosic biomass. *Bioresour. Technol.* **2016**, *200*, 971-980.
(15) Thoresen, P.P.; Matsakas, L.; Rova, U., and Christakopoulos, P., Recent advances in organosolv fractionation: Towards biomass fractionation technology of the future. *Bioresour. Technol.* **2020**, *306*, 123189.
(16) Lali, A.M.; Varavadekar, J.S., and Wadekar, P.C., *Process for fractionation of biomass* **2011**.
(17) Grande, P.M.; Viell, J.; Theyssen, N.; Marquardt, W.; Dominguez de Maria, P., and Leitner, W., Fractionation of lignocellulosic biomass using the OrganoCat process. *Green Chem.* **2015**, *17*, 3533-3539.
(18) Carneiro, A.P.; Rodríguez, O., and Macedo, E.A., Dissolution and fractionation of nut shells in ionic liquids. *Bioresour. Technol.* **2017,** *227*, 188-196.
(19) Yoo, C.G., *Pretreatment and fractionation of lignocellulosic biomass for production of biofuel and value-added products*. **2012**, Iowa State University.
(20) Mussatto, S.I. and Dragone, G.M., Chapter 1 - Biomass Pretreatment, Biorefineries, and Potential Products for a Bioeconomy Development, in *Biomass Fractionation Technologies for a Lignocellulosic Feedstock Based Biorefinery*. **2016**, Elsevier: Amsterdam. p. 1-22.
(21) Romero, I.; Ruiz, E., and Castro, E., Chapter 10 - Pretreatment With Metal Salts A2 - Mussatto, Solange I, in *Biomass Fractionation Technologies for a Lignocellulosic Feedstock Based Biorefinery*. **2016**, Elsevier: Amsterdam. p. 209-227.
(22) Santos, J.C.; Antunes, F.A.F.; Cunha, M.A.A.; Milessi, T.S.S.; Dussán, K.J.; Silva, D.D.V., and da Silva, S.S., Chapter 9 - Biomass Pretreatment With Oxalic Acid for Value-Added Products A2 - Mussatto, Solange I, in *Biomass Fractionation Technologies for a Lignocellulosic Feedstock Based Biorefinery*. **2016**, Elsevier: Amsterdam. p. 187-208.
(23) Shuddhodana; Mohnot, D.; Biswas, R., and Bisaria, V.S., Chapter 23 - Enzymatic Hydrolysis of Lignocellulosic Residues A2 - Mussatto, Solange I, in *Biomass Fractionation Technologies for a Lignocellulosic Feedstock Based Biorefinery*. **2016**, Elsevier: Amsterdam. p. 543-560.
(24) Wikandari, R.; Millati, R., and Taherzadeh, M.J., Chapter 12 - Pretreatment of Lignocelluloses With Solvent N-Methylmorpholine N-oxide A2 - Mussatto, Solange I, in *Biomass Fractionation Technologies for a Lignocellulosic Feedstock Based Biorefinery*. **2016**, Elsevier: Amsterdam. p. 255-280.
(25) Xu, J.K. and Sun, R.C., Chapter 19 - Recent Advances in Alkaline Pretreatment of Lignocellulosic Biomass A2 - Mussatto, Solange I, in *Biomass Fractionation Technologies for a Lignocellulosic Feedstock Based Biorefinery*. **2016**, Elsevier: Amsterdam. p. 431-459.
(26) Zhang, C.; Gleisner, R.; Houtman, C.J.; Pan, X., and Zhu, J.Y., Chapter 22 - Sulfite Pretreatment to Overcome the Recalcitrance of Lignocelluloses for Bioconversion of

Woody Biomass A2 - Mussatto, Solange I, in *Biomass Fractionation Technologies for a Lignocellulosic Feedstock Based Biorefinery*. **2016**, Elsevier: Amsterdam. p. 499-541.
(27) Zhang, J.; Cai, D.; Qin, Y.; Liu, D., and Zhao, X., High value-added monomer chemicals and functional bio-based materials derived from polymeric components of lignocellulose by organosolv fractionation. *Biofuel Bioprod. Biorefin.* **2020**, *14*, 371-401.
(28) Cheng, F.; Sun, J.; Wang, Z.; Zhao, X., and Hu, Y., Organosolv fractionation and simultaneous conversion of lignocellulosic biomass in aqueous 1,4-butanediol/acidic ionic-liquids solution. *Ind. Crops. Prod.* **2019**, *138*, 111573.
(29) Polavarapu, P.L. and Ewig, C.S., Ab Initio computed molecular structures and energies of the conformers of glucose. *J. Comput. Chem.* **1992**, *13*, 1255-1261.
(30) Kroon-Batenburg, L.M.J. and Kroon, J., Solvent effect on the conformation of the hydroxymethyl group established by molecular dynamics simulations of methyl-β-D-glucoside in water. *Biopolymers* **1990**, *29*, 1243-1248.
(31) van Eijck, B.P.; Hooft, R.W.W., and Kroon, J., Molecular dynamics study of conformational and anomeric equilibria in aqueous D-glucose. *J. Phys. Chem.* **1993** *97*, 12093-12099.
(32) Heiner, A.P. and Teleman, O., Interface between Monoclinic Crystalline Cellulose and Water: Breakdown of the Odd/Even Duplicity. *Langmuir* **1997**, *13*, 511-518.
(33) Heiner, A.P.; Kuutti, L., and Teleman, O., Comparison of the interface between water and four surfaces of native crystalline cellulose by molecular dynamics simulations. *Carbohydr. Res.* **1998**, *306*, 205-220.
(34) Matthews, J.F.; Himmel, M.E., and Brady, J.W., Simulations of the Structure of Cellulose, in *Computational Modeling in Lignocellulosic Biofuel Production*. **2010**, American Chemical Society. p. 17-53.
(35) Matthews, J.F.; Beckham, G.T.; Bergenstråhle-Wohlert, M.; Brady, J.W.; Himmel, M.E., and Crowley, M.F., Comparison of Cellulose Iβ Simulations with Three Carbohydrate Force Fields. *J. Chem. Theory Comp.* **2012**, *8*, 735-748.
(36) Matthews, J.F.; Bergenstråhle, M.; Beckham, G.T.; Himmel, M.E.; Nimlos, M.R.; Brady, J.W., and Crowley, M.F., High-Temperature Behavior of Cellulose I. *J. Phys. Chem. B* **2011**, *115*, 2155-2166.
(37) Hadden, J.A.; French, A.D., and Woods, R.J., Unraveling Cellulose Microfibrils: A Twisted Tale. *Biopolymers* **2013**, *99*, 746-756.
(38) Petridis, L.; O'Neill, H.M.; Johnsen, M.; Fan, B.; Schulz, R.; Mamontov, E.; Maranas, J.; Langan, P., and Smith, J.C., Hydration Control of the Mechanical and Dynamical Properties of Cellulose. *Biomacromolecules* **2014**, *15*, 4152-4159.
(39) Matthews, J.F.; Skopec, C.E.; Mason, P.E.; Zuccato, P.; Torget, R.W.; Sugiyama, J.; Himmel, M.E., and Brady, J.W., Computer simulation studies of microcrystalline cellulose Iβ. *Carbohydr. Res.* **2006**, *341*, 138-152.
(40) Yui, T.; Nishimura, S.; Akiba, S., and Hayashi, S., Swelling behavior of the cellulose Iβ crystal models by molecular dynamics. *Carbohydr. Res.* **2006** *341*, 2521-2530.
(41) Youssefian, S. and Rahbar, N., Molecular Origin of Strength and Stiffness in Bamboo Fibrils. *Sci. Rep.* **2015**, *5*, 11116.
(42) Silveira, R.L.; Stoyanov, S.R.; Gusarov, S.; Skaf, M.S., and Kovalenko, A., Plant Biomass Recalcitrance: Effect of Hemicellulose Composition on Nanoscale Forces that Control Cell Wall Strength. *J. Am. Chem. Soc.* **2013**, *135*, 19048-19051.
(43) Berglund, J.; Angles d'Ortoli, T.; Vilaplana, F.; Widmalm, G.; Bergenstråhle-Wohlert, M.; Lawoko, M.; Henriksson, G.; Lindström, M., and Wohlert, J., A molecular dynamics study of the effect of glycosidic linkage type in the hemicellulose backbone on the molecular chain flexibility. *Plant J.* **2016**, *88*, 56-70.

(44) Sauter, J. and Grafmüller, A., Solution Properties of Hemicellulose Polysaccharides with Four Common Carbohydrate Force Fields. *J. Chem. Theory Comp.* **2015**, *11*, 1765-1774.
(45) Durbeej, B. and Eriksson, L.A., *A Density Functional Theory Study of Coniferyl Alcohol Intermonomeric Cross Linkages in Lignin - Three-Dimensional Structures, Stabilities and the Thermodynamic Control Hypothesis*, in *Holzforschung*. **2003**. p. 150.
(46) Sawada, D.; Nishiyama, Y.; Petridis, L.; Parthasarathi, R.; Gnanakaran, S.; Forsyth, V.T.; Wada, M., and Langan, P., Structure and dynamics of a complex of cellulose with EDA: insights into the action of amines on cellulose. *Cellulose* **2013**, *20*, 1563-1571.
(47) Durbeej, B.; Wang, Y.-N., and Eriksson, L.A., Lignin Biosynthesis and Degradation — a Major Challenge for Computational Chemistry, in *High Performance Computing for Computational Science — VECPAR 2002: 5th International Conference Porto, Portugal, June 26–28, 2002 Selected Papers and Invited Talks*, J.M.L.M. Palma, A.A. Sousa, J. Dongarra, and V. Hernández, Editors. **2003**, Springer Berlin Heidelberg: Berlin, Heidelberg. p. 137-165.
(48) Besombes, S. and Mazeau, K., The cellulose/lignin assembly assessed by molecular modeling. Part 1: adsorption of a threo guaiacyl beta-O-4 dimer onto a Ibeta cellulose whisker. *Plant. Physiol. Biochem.* **2005,** *43*, 299-308.
(49) Besombes, S. and Mazeau, K., The cellulose/lignin assembly assessed by molecular modeling. Part 2: seeking for evidence of organization of lignin molecules at the interface with cellulose. *Plant Physiol. Biochem.* **2005**, *43*, 277-286.
(50) Kumar, R.; Bhagia, S.; Smith, M.D.; Petridis, L.; Ong, R.G.; Cai, C.M.; Mittal, A.; Himmel, M.H.; Balan, V.; Dale, B.E.; Ragauskas, A.J.; Smith, J.C., and Wyman, C.E., Cellulose–hemicellulose interactions at elevated temperatures increase cellulose recalcitrance to biological conversion. *Green Chem.* **2018**, *20*, 921-934.
(51) Yang, H.; Watts, H.D.; Gibilterra, V.; Weiss, T.B.; Petridis, L.; Cosgrove, D.J., and Kubicki, J.D., Quantum Calculations on Plant Cell Wall Component Interactions. *Interdiscip. Sci.* **2018**, *11*, 485–495.
(52) Petridis, L. and Smith, J.C., A molecular mechanics force field for lignin. *J. Comp. Chem.* **2009**, *30*, 457-467.
(53) Petridis, L. and Smith, J.C., Cellulosic ethanol: progress towards a simulation model of lignocellulosic biomass. *J. Phys. Conf. Ser.* **2008**, *125*, 012055.
(54) Petridis, L.; Schulz, R., and Smith, J.C., Simulation Analysis of the Temperature Dependence of Lignin Structure and Dynamics. *J. Am. Chem. Soc.* **2011**, *133*, 20277-20287.
(55) Hong, L.; Petridis, L., and Smith, J.C., Biomolecular Structure and Dynamics with Neutrons: The View from Simulation. *Isr. J. Chem.* **2014**, *54*, 1264-1273.
(56) Petridis, L. and Smith, J.C., Conformations of Low-Molecular-Weight Lignin Polymers in Water. *ChemSusChem* **2016**, *9*, 289-295.
(57) Petridis, L.; Pingali, S.V.; Urban, V.; Heller, W.T.; O'Neill, H.M.; Foston, M.; Ragauskas, A., and Smith, J.C., Self-similar multiscale structure of lignin revealed by neutron scattering and molecular dynamics simulation. *Phys. Rev. E* **2011**, *83*, 061911.
(58) Vermaas, J.V.; Petridis, L.; Qi, X.; Schulz, R.; Lindner, B., and Smith, J.C., Mechanism of lignin inhibition of enzymatic biomass deconstruction. *Biotechnol. Biofuels* **2015**, *8*, 217.
(59) Langan, P.; Petridis, L.; O'Neill, H.M.; Pingali, S.V.; Foston, M.; Nishiyama, Y.; Schulz, R.; Lindner, B.; Hanson, B.L.; Harton, S.; Heller, W.T.; Urban, V.; Evans, B.R.; Gnanakaran, S.; Ragauskas, A.J.; Smith, J.C., and Davison, B.H., Common processes drive the thermochemical pretreatment of lignocellulosic biomass. *Green Chem.* **2014**, *16*, 63-68.

(60) Sangha, A.K.; Petridis, L.; Smith, J.C.; Ziebell, A., and Parks, J.M., Molecular simulation as a tool for studying lignin. *Environ. Prog. Sustain. Energy* **2012**, *31*, 47-54.
(61) Schulz, R.; Lindner, B.; Petridis, L., and Smith, J.C., Scaling of Multimillion-Atom Biological Molecular Dynamics Simulation on a Petascale Supercomputer. *J. Chem. Theory Comp.* **2009**, *5*, 2798-2808.
(62) Lindner, B.; Petridis, L.; Schulz, R., and Smith, J.C., Solvent-Driven Preferential Association of Lignin with Regions of Crystalline Cellulose in Molecular Dynamics Simulation. *Biomacromolecules* **2013**, *14*, 3390-3398.
(63) Pingali, S.V.; O'Neill, H.M.; Nishiyama, Y.; He, L.; Melnichenko, Y.B.; Urban, V.; Petridis, L.; Davison, B., and Langan, P., Morphological changes in the cellulose and lignin components of biomass occur at different stages during steam pretreatment. *Cellulose* **2014**, *21*, 873-878.
(64) Aguilera-Segura, S.M.; Bossu, J.; Corn, S.; Trens, P.; Mineva, T.; Le Moigne, N., and Di Renzo, F., Synergistic sorption of mixed solvents in wood cell walls: experimental and theoretical approach. *Macromol. Symp.* **2019**, *386*, 1900022.
(65) Wang, Q.; Xiao, S.; Shi, S.Q., and Cai, L., Mechanical property enhancement of self-bonded natural fiber material via controlling cell wall plasticity and structure. *Mater. Des.* **2019**, *172*, 107763.
(66) Samyn, P., Wetting and hydrophobic modification of cellulose surfaces for paper applications. *J. Mater. Sci.*, **2013**. 48(19): p. 6455-6498.
(67) Stenius, P., Macromolecular, surface and colloid chemistry, in *Papermaking Science and Technology, Book 3. Forest Products Chemistry.* P. Stenius, J. Gullichsen, and H. Paulapuro, Editors. **2000**, PublisherFapet Oy: Jyväskylä. p. 173-278.
(68) Chang, S.; Quignard, F.; Di Renzo, F., and Clair, B., Solvent polarity and internal stresses control the swelling behavior of green wood during dehydration in organic solution. *BioResources* **2012**, *7*, 2418-2430.
(69) Lai, C.; Tu, M.; Li, M., and Yu, S., Remarkable solvent and extractable lignin effects on enzymatic digestibility of organosolv pretreated hardwood. *Bioresour. Technol.* **2014**, *156*, 92-99.
(70) Houtman, C.J. and Atalla, R.H., Cellulose-Lignin Interactions (A Computational Study). *Plant Physiol.* **1995**, *107*, 977-984.
(71) Charlier, L. and Mazeau, K., Molecular Modeling of the Structural and Dynamical Properties of Secondary Plant Cell Walls: Influence of Lignin Chemistry. *J. Phys. Chem. B* **2012**, *116*, 4163-4174.
(72) Smith, M.D.; Mostofian, B.; Cheng, X.; Petridis, L.; Cai, C.M.; Wyman, C.E., and Smith, J.C., Cosolvent pretreatment in cellulosic biofuel production: effect of tetrahydrofuran-water on lignin structure and dynamics. *Green Chem.* **2016**, *18*, 1268-1277.
(73) Smith, M.D.; Petridis, L.; Cheng, X.; Mostofian, B., and Smith, J.C., Enhanced sampling simulation analysis of the structure of lignin in the THF-water miscibility gap. *Phys. Chem. Chem. Phys.* **2016**, *18*, 6394-6398.
(74) Vasudevan, V. and Mushrif, S.H., Insights into the solvation of glucose in water, dimethyl sulfoxide (DMSO), tetrahydrofuran (THF) and N,N-dimethylformamide (DMF) and its possible implications on the conversion of glucose to platform chemicals. *RSC Adv.* **2015**, *5*, 20756-20763.
(75) Mostofian, B.; Cai, C.M.; Smith, M.D.; Petridis, L.; Cheng, X.; Wyman, C.E., and Smith, J.C., Local Phase Separation of Co-solvents Enhances Pretreatment of Biomass for Bioenergy Applications. *J. Am. Chem. Soc.* **2016**, *138*, 10869-10878.

(76) Smith, M.D.; Cheng, X.; Petridis, L.; Mostofian, B., and Smith, J.C., Organosolv-Water Cosolvent Phase Separation on Cellulose and its Influence on the Physical Deconstruction of Cellulose: A Molecular Dynamics Analysis. *Sci. Rep.* **2017**, *7*, 14494.
(77) Ciesielski, P.N.; Pecha, M.B.; Lattanzi, A.M.; Bharadwaj, V.S.; Crowley, M.F.; Bu, L.; Vermaas, J.V.; Steirer, K.X., and Crowley, M.F., Advances in Multiscale Modeling of Lignocellulosic Biomass. *ACS Sustain. Chem. Eng.* **2020**, *8*, 3512-3531.
(78) Petridis, L. and Smith, J.C., Molecular-level driving forces in lignocellulosic biomass deconstruction for bioenergy. *Nat. Rev. Chem.*, **2018**, *2*, 382-389.
(79) Mostofian, B.; Petridis, L., and Cai, C.M., Exploring Molecular Mechanisms of Cosolvent Enhanced Biomass Deconstruction: An Overview of Recent Progress, in *Understanding Lignocellulose: Synergistic Computational and Analytic Methods*. **2019**, American Chemical Society. p. 103-117.
(80) Pingali, S.V.; Smith, M.D.; Liu, S.-H.; Rawal, T.B.; Pu, Y.; Shah, R.; Evans, B.R.; Urban, V.S.; Davison, B.H.; Cai, C.M.; Ragauskas, A.J.; O'Neill, H.M.; Smith, J.C., and Petridis, L., Deconstruction of biomass enabled by local demixing of cosolvents at cellulose and lignin surfaces. *Proc. Natl. Acad. Sci. U.S.A.* **2020**, *117*, 16776-16781.
(81) Patri, A.S.; Mostofian, B.; Pu, Y.; Ciaffone, N.; Soliman, M.; Smith, M.D.; Kumar, R.; Cheng, X.; Wyman, C.E.; Tetard, L.; Ragauskas, A.J.; Smith, J.C.; Petridis, L., and Cai, C.M., A Multifunctional Cosolvent Pair Reveals Molecular Principles of Biomass Deconstruction. *J. Am. Chem. Soc.* **2019**, *141*, 12545-12557.
(82) Kahlen, J.; Masuch, K., and Leonhard, K., Modelling cellulose solubilities in ionic liquids using COSMO-RS. *Green Chem.* **2010**, *12*, 2172-2181.
(83) Gomes, T.C.F. and Skaf, M.S., Cellulose-Builder: A toolkit for building crystalline structures of cellulose. *J. Comp. Chem.* **2012**, *33*, 1338-1346.
(84) Pettersen, R.C., The Chemical Composition of Wood, in *The Chemistry of Solid Wood*. **1984**, American Chemical Society. p. 57-126.
(85) Abraham, M.J.; Murtola, T.; Schulz, R.; Páll, S.; Smith, J.C.; Hess, B., and Lindahl, E., GROMACS: High performance molecular simulations through multi-level parallelism from laptops to supercomputers. *SoftwareX* **2015**, *1–2*, 19-25.
(86) Bekker, H.; Berendsen, H.; Dijkstra, E.; Achterop, S.; Van Drunen, R.; Van der Spoel, D.; Sijbers, A.; Keegstra, H.; Reitsma, B., and Renardus, M., Gromacs: A parallel computer for molecular dynamics simulations, in *Physics computing '92*, R. DeGroot and J. Nadrchal, Editors. **1993**, World Scientific Publishing: Singapore. p. 252-256.
(87) Berendsen, H.J.C.; van der Spoel, D., and van Drunen, R., GROMACS: A message-passing parallel molecular dynamics implementation. *Comp. Phys. Commun.* **1995**, *91*, 43-56.
(88) Van Der Spoel, D.; Lindahl, E.; Hess, B.; Groenhof, G.; Mark, A.E., and Berendsen, H.J.C., GROMACS: Fast, flexible, and free. *J. Comp. Chem.* **2005**, *26*, 1701-1718.
(89) Páll, S.; Abraham, M.J.; Kutzner, C.; Hess, B., and Lindahl, E., Tackling Exascale Software Challenges in Molecular Dynamics Simulations with GROMACS, in *Solving Software Challenges for Exascale: International Conference on Exascale Applications and Software, EASC 2014, Stockholm, Sweden, April 2-3, 2014, Revised Selected Papers*, S. Markidis and E. Laure, Editors. **2015**, Springer International Publishing: Cham. p. 3-27.
(90) Jorgensen, W.L.; Chandrasekhar, J.; Madura, J.D.; Impey, R.W., and Klein, M.L., Comparison of simple potential functions for simulating liquid water. *J. Chem. Phys.* **1983**, *79*, 926-935.
(91) Dick, T.J. and Madura, J.D., Chapter 5 A Review of the TIP4P, TIP4P-Ew, TIP5P, and TIP5P-E Water Models, in *Annual Reports in Computational Chemistry*. **2005**, Elsevier. p. 59-74.

(92) Mark, P. and Nilsson, L., Structure and Dynamics of the TIP3P, SPC, and SPC/E Water Models at 298 K. *J. Phys. Chem. A* **2001**, *105*, 9954-9960.
(93) Guvench, O.; Greene, S.N.; Kamath, G.; Brady, J.W.; Venable, R.M.; Pastor, R.W., and Mackerell, A.D., Additive empirical force field for hexopyranose monosaccharides. *J. Comput. Chem.* **2008**. *29*, 2543-2564.
(94) Guvench, O.; Hatcher, E.R.; Venable, R.M.; Pastor, R.W., and Mackerell, A.D., CHARMM additive all-atom force field for glycosidic linkages between hexopyranoses. *J. Chem. Theory Comput.* **2009**, *5*, 2353–2370.
(95) van der Spoel, D.; van Maaren, P.J., and Caleman, C., GROMACS molecule & liquid database. *Bioinformatics* **2012**, *28*, 752-753.
(96) Eisenhaber, F.; Lijnzaad, P.; Argos, P.; Sander, C., and Scharf, M., The double cubic lattice method: Efficient approaches to numerical integration of surface area and volume and to dot surface contouring of molecular assemblies. *J. Comput. Chem.* **1995**, *16*, 273-284.
(97) Aguilera-Segura, S.M.; Di Renzo, F., and Mineva, T., Structures, intermolecular interactions, and chemical hardness of binary water–organic solvents: a molecular dynamics study. *J. Mol. Model.* **2018**, *24*, 292.
(98) Maurer, R.J.; Sax, A.F., and Ribitsch, V., Molecular simulation of surface reorganization and wetting in crystalline cellulose I and II. *Cellulose* **2013**, *20*, 25-42.
(99) Miyamoto, H.; Abdullah, R.; Tokimura, H.; Hayakawa, D.; Ueda, K., and Saka, S., Molecular dynamics simulation of dissociation behavior of various crystalline celluloses treated with hot-compressed water. *Cellulose* **2014**, *21*, 3203-3215.
(100) Goldmann, W.M.; Ahola, J.; Mikola, M., and Tanskanen, J., Solubility and fractionation of Indulin AT kraft lignin in ethanol-water media. *Sep. Purif. Technol.* **2019**, *209*, 826-832.

Graphical Table of Contents